



Politecnico di Bari

Repository Istituzionale dei Prodotti della Ricerca del Politecnico di Bari

A new video monitoring system in support of Coastal Zone Management at Apulia Region, Italy

This is a pre-print of the following article

Original Citation:

A new video monitoring system in support of Coastal Zone Management at Apulia Region, Italy / Valentini, Nico; Saponieri, Alessandra; Damiani, Leonardo. - In: OCEAN & COASTAL MANAGEMENT. - ISSN 0964-5691. - 142:(2017), pp. 122-135. [10.1016/j.ocecoaman.2017.03.032]

Availability:

This version is available at <http://hdl.handle.net/11589/108309> since: 2021-03-08

Published version

DOI:10.1016/j.ocecoaman.2017.03.032

Publisher:

Terms of use:

(Article begins on next page)



A new video monitoring system in support of Coastal Zone Management at Apulia Region, Italy

Nico Valentini^{*}, Alessandra Saponieri, Leonardo Damiani

Department of Civil, Environmental, Building Engineering and Chemistry, Technical University of Bari, Via E. Orabona, 4, 70125, Bari, Italy

ARTICLE INFO

Article history:

Received 25 October 2016

Received in revised form 14 March 2017

Accepted 31 March 2017

Available online xxx

Keywords:

Video monitoring

Apulian coastal management

Image processing

Intertidal bathymetry

ABSTRACT

New systems for video monitoring and surveillance of Apulian coasts (South-east of Italy) have been recently employed. The system design aims at obtaining a tool able to automatically perform image acquisition, image processing and dissemination of results on a web portal. In the present paper, the system implementation and video stations installation at two different sites are described. A new specific Shoreline Detection Model (SDM) has been developed, based on boundary extraction procedure from automatic segmented coastal area. In real time, processed images and shoreline maps are uploaded and made freely downloadable. Moreover, shoreline time variation analysis is available on user-selected transects in cross-shore direction. The SDM model validation is here presented at one location. Over a set of testing images, the pixel-based comparison between manually and automatically detected shorelines lead to a mean distance of about 1.17 pixel. Then, the reconstruction of intertidal bathymetry from video is reported and compared with topographical (d-RTK) field survey, in order to assess the system efficacy and accuracy in coastal area monitoring, resulting in a mean RMS error overall the transects investigated equal to 0.025 m.

© 2016 Published by Elsevier Ltd.

1. Introduction

Nowadays, our territories are heavily exposed to several hazards weakening their environmental quality and sustainability. The exploitation of natural resources must be carefully planned and managed, properly focused on a reliable risk impact assessment. Several models have been proposed in order to quantify the environmental, social and economic impacts of natural hazards, through the definition of state indicators (e.g. Archetti et al., 2016; Jimenez et al., 2007; Valipour, 2016; Valipour et al., 2017). Coastal zone are particularly vulnerable ecosystems, highly suffering from urbanization and human activities effects. For this reason, Integrated Coastal Zone Management (ICZM) is required by means of a reliable, understandable and timely knowledge of processes affecting coastal hazards, getting both decision makers and local communities involved, in order to gain a broad-based support and public participation. A people-centred information system focused on reaching local communities risk perceptions is useful in order to develop a so-called participatory monitoring (Estrella and Gaventa, 1998; Nagy et al., 2015) aimed to use stakeholders' and local communities' experience, integrated with scientific knowledge, in developing models able to support environmental phenomena analysis and define a scale of actions priorities.

In this perspective, coastal management retains a crucial importance in order to shape economic and social assets, especially for places with large sea resources. To accomplish such an evidently powerful scope, coastal monitoring operating surveys have been es-

tablished to represent a priority stage, in order to collect data useful for the study of hydrodynamic processes and morphological evolution, or defence as traditional and innovative mitigation works (Damiani et al., 2011; Saponieri and Damiani, 2015) effects and efficacy. Specifically, in order to follow beach evolution and storms response, nourishments and dredging activities (Kroon et al., 2007), prior variables to be monitored are shoreline position and topo-bathymetric data.

To date, video monitoring technique represents an alternative solution to the traditional approaches, with low installation and management costs. The inadequacy in measurements frequency of shoreline position and its time variability, using i.e. cross-shore profiles surveys and aerial photographs, makes the land-based video platforms based on digital image-processing techniques an optimal instrument to derive objective shoreline position (Boak and Turner, 2005). Such a method allows to acquire and share long-term and continuous information, even in real time, with both larger temporal and spatial sampling frequency. A limit is the data storage, which could be too much consuming for remote sites. With regard to this constraint, a sharp compromise is reached by introducing *Timex images*, since the first Argus monitoring system, which create an averaging of the collected snapshots, acted to easily represent the average energy dissipation of the random wave field over beach. Long-time series of Timex and Day-Timex images provide excellent, low-cost datasets of morphodynamic variability over time scales from days to decades (Holman and Stanley, 2007). Variance images are generally stored and presented in terms of standard deviations (SIGMA) rather than real mathematical variance, but the shorter name is retained for convenience. Several techniques are proposed to process images in order to derive several information about morphodynamic as well hydrodynamic processes (i.e. Aarninkhof et al., 2005; Holman et al., 2013;

^{*} Corresponding author.

Email addresses: nico.valentini@poliba.it (N. Valentini); alessandra.saponieri@poliba.it (A. Saponieri); leonardo.damiani@poliba.it (L. Damiani)

Jimenez et al., 2007; Plant and Holman, 1997; Radermacher et al., 2014; Sembiring, 2015; Simarro et al., 2015; Stockdon et al., 2006).

The first and main application concerns with shoreline detection from oblique or rectified images, which allows following long-term coastline movement as well as the short-term response to storms. The shoreline extraction from images is based on discriminating sea from sand, requiring firstly image-processing procedures, in order to identify the shoreline contour, whose appearance characteristics may vary as far as the beach morphodynamic environment.

In earlier studies (Plant and Holman, 1997), the white band pattern discernible from the Timex grayscale images, corresponding to the shore-parallel swash motions, has been identified and defined as the ShoreLine Intensity Maximum (SLIM). The SLIM method is revealed highly sensitive to the variations of the surf similarity parameter, also in reflective beaches, where the swash dissipation signature is strongly marked (Plant et al., 2009). The analysis of full colour images allows obtaining more information from video recordings but, at the same time, the investigation and the improvement of new techniques have become necessary. Turner et al. (2001) use the different reflectance properties of wet and dry regions in order to develop a new method, based on the identification of the divergence of red and blue pixels' intensities over cross-shore transects. Osorio et al. (2012) extract the shoreline contour by linking together six edge-detection techniques, based on a combination of statistical criteria forced with physical constraints (i.e. tidal cycle) over the spatially extension of the detection research area, deploying the Physical and Statistical Detection Model.

In full colour images processing the shoreline-mapping issue, based on RGB channels values analysis, could be faced with the use of a contour objective function aimed to define a threshold level within the region that bounds the shoreline. Such a contours detection is possible by partitioning an image into similar regions. An early approach (Kingston, 2003, Kingston et al., 2003) uses an opportunely trained Artificial Neural Networks (ANN) for the classification of land and water regions by defining the model output as a continuous variable with water and land samples having a value close to 0 and 1, respectively.

The actual Argus commercial systems, since the implementation of the so-called Intertidal Beach Mapper tool, use the Pixel Intensity Clustering (PIC) model. The model is applied on Timex images, in a specific Region Of Interest (ROI) by means of a discriminator function for differentiating two clusters (Aarninkhof, 2003; Aarninkhof et al., 2003). The efficiency of the algorithm, completely automatized by Uunk et al. (2010), is guaranteed by the application of the routine on the two-dimensional colour (Hue-Saturation) and luminance (Value-Value) domains, using the best contrast.

Vousdoukas et al. (2011) implement a data-driven automated procedure on SIGMA images over a ROI, using information retained by images histograms fitted on an ensemble function of a 2nd order polynomial and two Gaussian shape functions. Over a vector composed by more than 1000 images in their trials, the optimal threshold value is based on the minimum Root Mean Square Error (RMSE) between automatic and manual extracted shoreline contours. A three-layer ANN perceptron, trained by the Levenberg-Marquardt algorithm, is introduced by using the fitting functions parameters and the four histogram statistical moments as inputs (Vousdoukas et al., 2011). Compared to a priori threshold intensity value method, the ANN leads to a decrease in the average RMSE cross-shore locations and an increase of the overall data return rate.

A very similar approach, resulting in a highly performing automatic procedure, is described in Rigos et al. (2014). Differences between the two methods are related to functions used for histogram fitting and the ANN method. The Chebyshev polynomials are encompassed to approximate the histograms of grayscale variance images,

after segmentation thresholding-based process developed in Vousdoukas et al. (2011). Radial Basis Function (RBF) network is employed, where the number of polynomial coefficients defines the dimension of input space. A fuzzy c-means clustering analysis has been used for Radial Basis Function centres determination and the connection weights of the hidden nodes are calculated by using a steepest descent approach (Pedrycz, 1998; Rigos et al., 2014).

The above-mentioned techniques represent the most popular and overused methods. On the contrary, the segmentation and classification of the fundamental areas framed by typical coastal video monitoring station field of view has been rarely studied, and, to date, they could represent an alternative solution in order to eliminate the constraint due to the research of ROI area. A nearly contemporary work (Hoonhout et al., 2015) uses a semantic approach for the automatic pixels classification. Pre-defined set of classes, based on thousands of intrinsic and extrinsic pixel features, are defined and a supervised learning (SSVM) for class distinction is trained. Object-oriented analysis on low-tide images of Argus system has been tested in Quartel et al. (2006) for morphology segmentation, using maximum likelihood classification, based on manually labelled regions for defining a model of class prediction.

In Apulia region, beach video-monitoring is still at initial stages of development, mainly because of the relative high cost of commercial systems that has made the littoral video-monitoring difficult to be deployed and maintained for public institutions. In 2005, a video-monitoring station was installed at Alimini (Lecce) in South Italy (Damiani and Molfetta, 2008). The routine developed for Alimini coastal video-systems is a colour-based and user-assisted procedure, implemented in MATLAB environment, aimed at extracting shoreline position, run-up time series and beach slope variation (Lisi et al., 2011) from RGB colour coded Timex images. The routine, partially includes the code developed by Lau (1997). The large swash excursion occurring on very low sloped nearshore (around $1 \div 2\%$) as well as the presence of intertidal bars, lead to a large buffer area to process (around $\cong 1000$ pixel on the rectified image). For this reason, the routine needs to start with the definition of a ROI by the user. User must identify some reference points (regularly more than two to increase performance) in order to distinguish and segment sand and sea in the ROI area. The tool works by selecting connected groups of pixels whose colour are consistent with the user-selected reference pixels, with a predefined tolerance. A real time visual inspecting of the detected waterline is allowed. A suitable procedure enables to remove obstacles on the image frame, especially in summer (e.g. beach umbrellas, vehicles, etc.). It is mainly based on the interpolation of neighbouring pixels around the foreign objects, permitting its deletion. The main limit of such a procedure is that the shoreline extraction from image is not automatic, because the contour recognition in each single image must be initialized with some initial reference pixels selected by the user with a consequent increasing of processing time, and often in order to get better results, the tolerance level is changed for a colour similarity assimilation.

For this reason, the development of a new, efficient, almost completely automatic and low-cost system is fully justified. This has been achieved through the installation of a video-monitoring system, built upon calibrated non-metric IP surveillance cameras, able to accurately quantify coastal processes.

The paper describes a new video monitoring system deployed in 2015 in Apulia region (South Italy), aimed at supporting management and monitoring activities of coastal areas. Video stations are installed at two different sites, characterized by different geographic exposition and wave climate. The shoreline extraction and the data post processing are based on new algorithms automatically working on Timex images, providing a calculation of shoreline planimetric evolution and cross-shore profiles. Moreover, shoreline position maps

and its time variation on specific transects are published in quasi real time on a web site. The video system employed improves the actual available methodologies described above in the image analyses, shoreline extraction as well as results post-processing procedures. Specifically, the constraint of manually detecting a ROI area is overcome and the entire image is processed, by using only few seeds aimed at areas segmentation. The final segmented image is in the present work used for shoreline recognition, but the procedure can be easily extended for other purposes, in order to detect significant objects or other coastal specific zones (i.e. dunes, intertidal beach extension, etc.). Moreover, all implemented routines work automatically, without constant operator interventions. The images, indeed, are automatically processed and the shoreline contour directly extracted from images and then analysed. Cross-shore shoreline time variations on specific transects are available after an automatic process of geo-rectification, made with respect to the sea level recorded by the nearest tide-gauge.

The shoreline detection model has been firstly calibrated and validated at the previous coastal video monitoring station installed at Alimini (Lecce, Italy). After the installation and the calibration of the two systems in 2015, the shoreline extraction code has been tested for the new sites. In the present paper, the intertidal bathymetry derived from video analysis and the shorelines comparison in pixel space at Porto Cesareo will be presented.

2. System description

The new system is included in a broader Apulia meteo-oceanographic monitoring network, active since 2006 and managed by the local Apulian Basin Authority. The monitoring network includes 2 wave buoys, 4 tide stations and 6 anemometric stations. The collected data are stored in a control centre in real time via GSM and they are freely available on the web portal <http://93.51.158.171/web/simop/home>.

The development of a new video monitoring system has required considerable efforts to ensure an efficient as well as easy-to-install system, able to automatically acquire and process images, with both low installation and management costs. Moreover, a user-friendly, Java based web interface has been built to contribute to the distribution of video-analysis results and gain a broad-based support with public participation.

The system, briefly described in the following sections, is mainly composed by 3 modules. The outline of the processes is detached in Fig. 1 and includes image acquisition, image pre/post processing for shoreline detection and publication of the results on a web-site, accessible from the Meteo-Oceanographic Information System (SIMOP) of the Basin Authority of Apulia Region. The tasks are executed and automatized by using Python scripting, partially including libraries from OpenCV, flamingo-openeearth and Gdal/OSR.

2.1. Image acquisition

The acquisition system is implemented by using state of the art autonomous IP cameras, placed on-site, detached from archiving/processing remote server or laptop, disjoining the image post-processing from the acquisition and guaranteeing a decentralized framework. By this way, the acquisition phase could be preserved during components maintenance, by using substituted hardware. Images are stored on both local low-cost (Unix-based operating system) with available local Hard-Drive copy and remote servers. The web-portal is supplied by server storage via rest call. The use of low-cost router, dual-band 4G/3G sim cards enable a secure and, depending on the network coverage (signal strength), fast connection. Such a source, combined with a stable power supply serving server with remote controls features determine an increment of system efficiency, particularly for far-field system location.

2.2. Geometry of cameras

The transformation of the image coordinates to world coordinates involves 3 main steps, which can be summarized in: (i) intrinsic calibration, where the internal camera parameters are determined in laboratory, or even in field; (ii) the proper image correction, which aims to correct the relatively large image distortions induced by internal camera optics and (iii) image rectification to transform oblique images into vertically equivalent images (rectified images).

Most of the commercial cameras undertake an amount of manufacturer distortions, which must be corrected. The intrinsic calibration has been performed together with cameras installation, accounting for the following parameters: focal length, principal points, distortions with radial at 6° order and tangential components, neglecting skew. For visible cameras, the mostly used in video monitoring systems, ordinary chessboards are used for this task (Bouguet, 2004; Bradski and Kaehler, 2008; Wolf and Dewitt, 2000; Zhang, 2000). The correction process is automatically applied on each image after its storage, just before the geo-rectification process. The model used to describe the internal matrix and the distortion model in matricial form, is as follows (Eq. (1)):

$$\begin{bmatrix} u \\ v \\ w \end{bmatrix} = \begin{bmatrix} f_x & 0 & c_x \\ 0 & f_y & c_y \\ 0 & 0 & 1 \end{bmatrix} \begin{bmatrix} x'' \\ y'' \\ z'' \end{bmatrix} = K \begin{bmatrix} x'' \\ y'' \\ z'' \end{bmatrix} \quad (1)$$

where u , v and z represent the point coordinates in the distorted system; f_x and f_y the camera focal lengths in x and y -directions, respectively, and c_x , c_y are the optical centre positions expressed in pixel coordinates. The matrix K containing these four parameters is referred to as the Camera Matrix. The vector (x'', y'', z'') corresponds

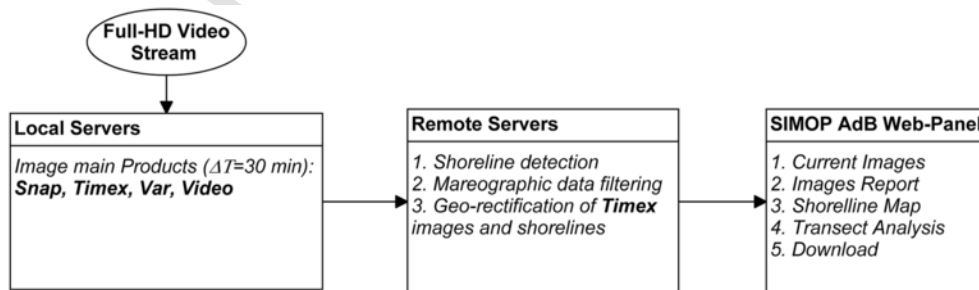


Fig. 1. Process outline of the main tasks of new coastal video monitoring system.

to the normalized point with radial and tangential distortion numerically defined as (Eqs. (2) and (3)):

$$\begin{aligned} x'' &= x' (1 + k_1 r^2 + k_2 r^4 + k_3 r^6) \\ &\quad + 2 p_1 x' y' + p_2 (r^2 + 2 x'^2) \\ y'' &= y' (1 + k_1 r^2 + k_2 r^4 + k_3 r^6) \\ &\quad + 2 p_2 x' y' + p_1 (r^2 + 2 y'^2) \end{aligned} \quad (2)$$

$$r^2 = x'^2 + y'^2 \quad (3)$$

where $x' = x/z$ and $y' = y/z$ are normalized undistorted coordinates of image point; k_1, k_2, k_3 are radial distortion coefficients. While p_1 and p_2 are the tangential distortion coefficients considered. Higher-order coefficients and thin prism distortion are not considered in this context. In Equation (1) w is explained by the use of homography coordinate system and it is equal to z'' . For images rectification the so-called external (or extrinsic) parameters, as camera global coordinates and orientation, are necessary. The pinhole camera model (Fig. 2) has been considered for the external calibration, which is computed in order to transform the undistorted image coordinates in the global ones. Such a task has been typically solved in many photogrammetric and coastal video applications by using the well-known Direct Linear Transform (DLT) algorithm, by using at least 3–4 Ground Control Points (GCPs) and relative image coordinates correspondences, also when including focal length (Holland et al., 1997). There are, though, several simplifications to the problem, which turns into an extensive list of different algorithms that improve the accuracy of the DLT (Penate-Sanchez et al., 2013), once known the internal parameters. This is the so-called Perspective- n -Point problem, for which three point correspondences are sufficient in its minimal version (Gao et al., 2003), while solutions to the over-constrained problem with $n > 3$ point correspondences exist as iterative (Horaud et al., 1997; Lu et al., 2000) and non-iterative solutions (Ansar and Daniilidis, 2003; Fiore, 2001). Here an iterative solver is applied by minimizing the sum of the re-projection errors, which corresponds to the accumulated squared distance between the 3D point projection and its measured 2d coordinates. The minimization is applied by using Levenberg-Marquardt algorithm, hence the 3×4 perspective transformation P , Eq. (4) is calculated as follows:

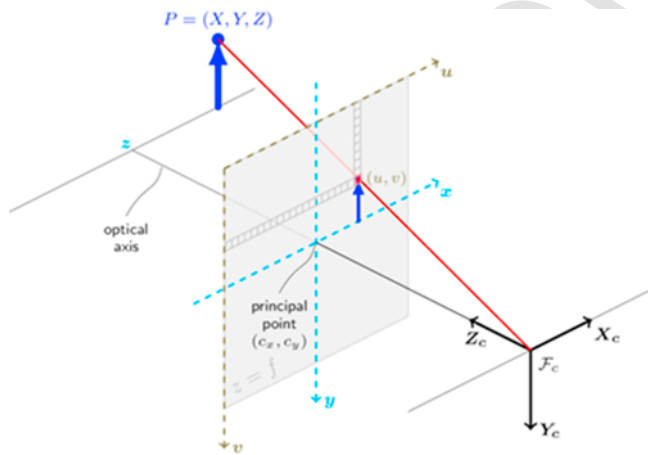


Fig. 2. Sketch of a Pinhole camera model (from OpenCV, 2016).

$$P = K R [I|C] \quad (4)$$

where I is the identity matrix, C and R are the translation vector and rotation matrix, respectively, of the camera Centre of View (CoV). The R retains information of the effective orientation of the CoV with respect to the Cartesian axes. The joint rotation-translation matrix $[R|C]$ is called matrix of extrinsic parameters.

Sea levels have been used as reference elevation value for geo-rectification procedure. In order to avoid the use of such raw data, not yet validated, a quasi-real-time filter is implemented in MATLAB environment and automatized by Python scripting, in order to eliminate outliers and spikes (IOC, 2006).

2.3. Image displacement assessment

The considerable meteorological variability, due to i.e. strong wind, heavy rain, or even hailstorm, human inadvertences, thermal expansion and mechanical factors could lead to unexpected changes of the precise cameras CoV location, and this may imply the loss of information/fault in the geo-rectification procedure. The definition of a procedure in order to correct the perspective transformation P has been demonstrated to be extremely important in order to reduce these significant geo-rectification errors (Holman and Stanley, 2007). Consequently, the availability of real-time and/or one-off controls is desirable also in order to keep preserved the external calibration parameters as long as possible.

A procedure, basically built on computer vision algorithms, also inspired by Vousdoukas et al. (2011), is defined in this context. In the following i) 5/6 snapshot images, taken at different illumination conditions at the time of external calibration, for which camera geometry is known, are selected and undistorted referred as set I_R ; ii) snapshot images, for which the image displacement has to be calculated, uniformly distributed over a day, are undistorted, in the number of 15 around, referred as set I_D . The SURF algorithm, which can be classified as a local features detector and descriptor, mostly used for image alignment or make 3d reconstructions (Bay et al., 2008), is then applied to both I_R and I_D . The characteristic feature points detected, outside those regions where fixed structures are framed, are manually masked/filtered out. Then the locations retrieval of matched points using SURF algorithm between the two data sets is performed and identical matched points are neglected. If the number of retrieved key-points matched in the previous step is greater than 10, the following tasks are applied.

A geometric transform estimator (Hartley and Zisserman, 2003) assuming a non-reflective similarity transformation, allows to remove outliers by using the RANSAC schema (Fischler and Bolles, 1981). Furthermore, the use of Procrustes analysis (Kendall, 1989), determines a linear transformation matrix M_{DR} between the points matched from the set I_D to best conform to those in the set I_R . The undistorted coordinates of the previous/original GCPs are transformed by applying the matrix M_{DR} . The mean values of the new GCPs are used for updating the external calibration and geo-rectification procedures.

The above described procedure does not consider high frequency oscillations, due, for instance, to wind turbulence. In this case, in fact, the wind-driven oscillation is considered to be compensated while the Timex is composed during the 10 min acquisition period, since a simple Snapshot is mostly used only for illustrative purposes. While drifting and camera angle changes (jumps) are not yet observed during a barely year monitoring period of the systems, unlike described in (Holman and Stanley, 2007; Vousdoukas et al., 2011).

2.4. The Shoreline Detection Model (SDM)

The Shoreline Detection Model (SDM) described in brief hereafter is the results of the boundary extraction from automatic segmented coastal area. Images recorded by video cameras are firstly pre-processed and prepared for the main processes, in order to bypass issues due to low/different illumination, contrast and to the presence of objects/algae or people on the swash area. A distribution of the popular software ImageJ, the Fiji software (Schindelin et al., 2012), embedded into the main routine, is used for this task. In this phase, the RGB images are transformed in CIELab color space and then processed by contrast enhancement and median filtering routines and, at the end, an edge preserving smoother is applied (Thévenaz et al., 2012).

Then, the main shoreline detection algorithm is implemented, inspired by the Global Probability of Boundary detector (Arbelaez et al., 2011), combined with segmentation steps based on detected boundaries procedures and then, on the colour properties recognition for intertidal bars detection and a parallel overall correction. In the present work the ROI area limits, widely adopted in literature, are removed to face regional morphological/urbanization properties due to the combination of both swash length seasonal differences and low cameras height. While small seeds pixel areas are introduced in order to cope mainly with the constrained segmentation on the Ultrametric Contour Map, using Voronoi metric space. It has been figured out that illumination and atmospheric dust/rain have a great influence on the Colour properties of those images. For the first time introduced in the work of Aarminkhof (2003), the luminance and hue-saturation domains colour properties are investigated in order to retrieve the relative spread of pixel intensities within each cluster and determine the best contrast. In the present work, a similar approach is applied by using the perceptually linear CIELab colorspace. The histograms of the masked image by two small seed areas (around 200 pixels) representative of the sea and sand pixel surfaces are calculated. The normalized Chi-Square histogram (Pele and Werman, 2010) distance (H_d) is, assumed to determine the best contrasting colour feature, between L and b , useful for the further processing. The ensemble of the processes is built on MATLAB software environment, taking advantage of efficient algorithms already available and addressed at solving such complex scheme architectures (Aarminkhof et al., 2003; Vousdoulas et al., 2011; Valipour et al., 2013). Then it is automatized by compiling a unique executable code in Matlab Compiler Runtime (2013a) (v8.1) on Linux 64bit, in order to guarantee a quick and secure distribution of the application.

The above described procedure, from the post processing to the shoreline extraction, is calibrated and validated on images recorded by the video system installed at Alimini. A dataset of 30 images, characterized by different illumination conditions, is used in order to calibrate the Global Probability of Boundary function. Another 30 images testing dataset allowed the model validation. In Fig. 3 an example of shoreline contour automatically detected by the calibrated model is reported and compared with the shoreline manually recognized. In the images, mostly characterized by quite straight shoreline in an optimal illumination condition, the sample dispersion, represented by the distance between the upper and lower quartiles, is very close to the median. Moreover, about the 30% of Alimini images, mostly relative to the further transects from the cameras, highlights the presence of outliers. Results also show that few images are characterized by a high standard deviation probably due to the SDM performance ambiguity in recognizing sharp bends along the shoreline, especially for transects placed far from the cameras.



Fig. 3. Example of comparison between manually (red dots) and automatic shoreline contours (blue dots) at Alimini shore. (For interpretation of the references to colour in this figure legend, the reader is referred to the web version of this article.)

2.5. Web-site

The possibility of sharing the results of coastal video-monitoring is quite promising, supporting professionals and coastal managers in morphological analysis. Furthermore, beach-users and stakeholders may be aware on actual beach state and relative evolution. This has led to the construction of a web-portal (<http://91.121.30.84/>), which includes the publication of results in a quasi-real time (Fig. 4).

The web-site is specifically built by using JavaScript and coded HTML, and it is a 1.0 version, released and included into the main Apulian Basin Authority coastal web-area (simopadb.dyndns.org/web/simop). It consists of 5 modules of different consultation tabs. The *Current images* tab is intended to list the last images produced at all the stations of the system, including those produced (Snap, Timex, STD and geo-rectified). The *Images Report* allows user to view thumbnails and download images, choosing interval and extremes date of a time period. The mapping of the geo-rectified shoreline over the rectified geo-referenced image is visible on *Shoreline map* tab, while the *Shoreline Transect Analysis* tool shows the cross-shore time variation of shoreline position with respect to a baseline on a user-specified transect on the oblique view (Fig. 4). The output data can be freely downloaded by the *Download* tab.

3. System application

Two new video monitoring systems are integrated in the Apulia Monitoring Network, at two different sites along the Apulian coast, Torre Canne (Fasano, Brindisi) and Torre Lapillo (Porto Cesareo, Lecce), which have been investigated for several years, to monitor the morphodynamic evolutionary trend for further analysis, by using video analysis (Fig. 5).

The stream of each camera is configured in such a way to have an acquisition cycle of 10 min with a frequency of 1 Hz, resulting in 600 images every half an hour. The sampling interval is 30 min. The main products produced and stored into the local servers are three fundamental types of images: Snapshot, Timex and Variance (Holman and Stanley, 2007). The transfer to a cloud server is granted by local router connectivity.

The remote pre- and post-processing tasks are applied once each new image is uploaded. Specifically, the SDM model is implemented

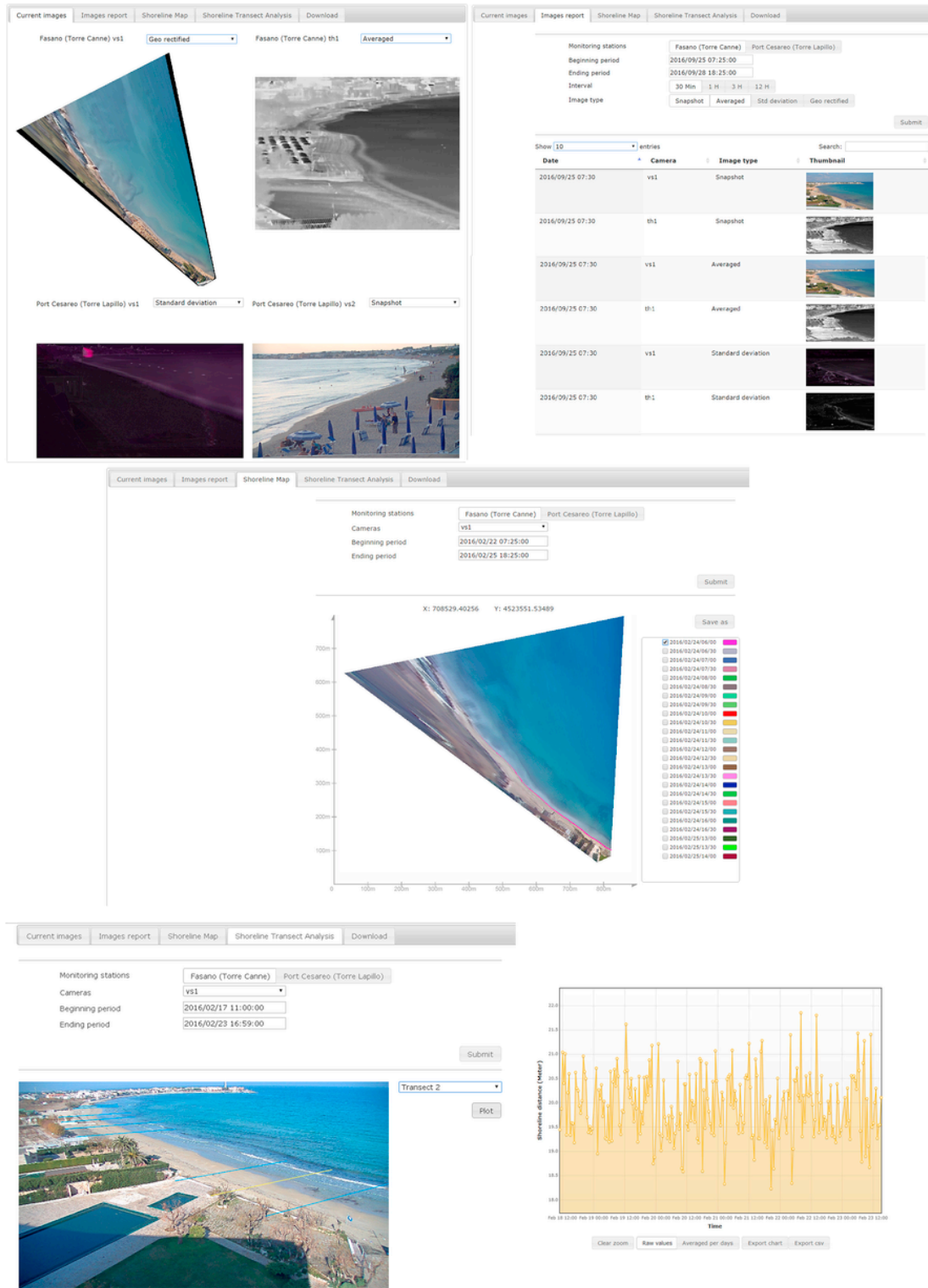


Fig. 4. Top: Current Images and Images Report tabs; Middle: Shoreline Map tab with an example of mapped shoreline on geo-rectified image (purple dotted lines); Bottom: Cross-shore transect user-selected (yellow) and an example of time variation of shoreline distance from the reference baseline. (For interpretation of the references to colour in this figure legend, the reader is referred to the web version of this article.)

on the Timex. Then the sea level data filter is executed, in order to obtain the reference elevation used for geo-rectification procedure applied on images as well as detected shoreline.

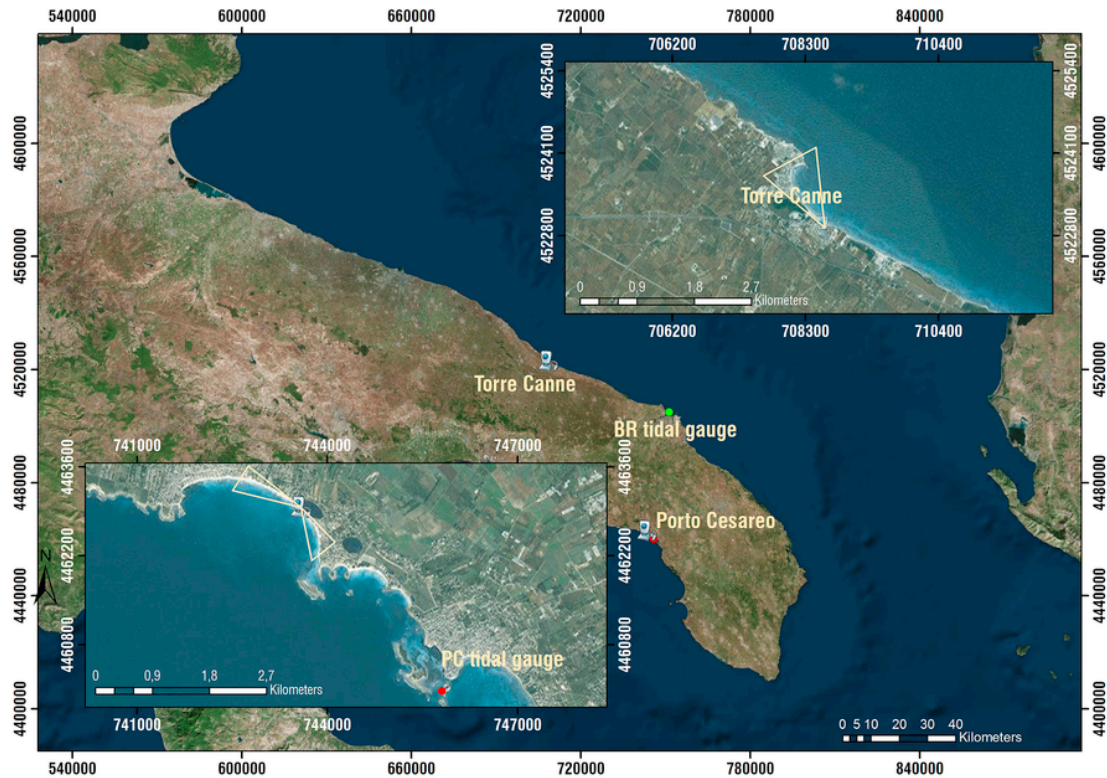


Fig. 5. New video monitoring stations installed at Apulia region: Camera locations and approximate Field of View (FoV). Nearest tidal buoys of Apulia monitoring network (red and green dots). (Grid coordinates: RDN2008/TM33). (For interpretation of the references to colour in this figure legend, the reader is referred to the web version of this article.)

3.1. Torre Canne, Fasano (Brindisi, Italy)

3.1.1. Study area

Torre Canne site represents an important thermal location for Apulia region, facing the Adriatic Sea. Beaches are characterized by medium grain size sand, according to Udden-Wentworth scale, with a mean diameter of the particle size distribution D_{50} and a D_{95} equal to 0.28 mm and 0.44 mm, respectively. The emerged beach is about $20 \div 50$ m wide, characterized by a steep berm with periodically vegetation encroachment. The wave climate in the area is moderate, with an annual significant wave height ranging from 0.5 m to 1.5 m for the 49.75% of wave observations in 1990–2007. Only the 0.16% of the measured wave heights exceeds 3.5 m. A peak period from 3 s to 7 s constitutes the 67.6% of observations. The wave climate is dominated by waves propagating from NNW for the 29.7% of the time, while a discrete contribute of the sector ESE occurs for about 18% (Petrillo, 2010). The great urbanization rate, mainly due to touristic activities, has been crucial in the negative sedimentary balance of the area (AdB-Puglia, 2015). Indeed, in the last decade, the analysis of long-term shoreline movements, highlights a global erosional trend, with maximum shoreline withdraws equal to about 10 m at few spots, which, recently, have become quite stable.

3.1.2. System implementation

At Torre Canne (TC) two IP network cameras are installed on a steel pole, which is fixed by brackets on parapet of a Hotel. The approximate orthometric height of the cameras is 23.4 m (ITALGEO 2005). In Fig. 6 the installed cameras are shown, and coastal stretch under investigation framed.

The system consists of one thermal (TC_{th}) and one visible (TC_{vs}) cameras, both faced NNW, with a Field of View (FoV) of 10° and

59.5° , respectively. The TC_{vs} is an Axis, Mod. Q1765-LE Network Camera, TC_{th} is an Axis, Mod. Q1931-E Thermal Network Camera. Both visible and thermal are outdoor-ready network cameras. The TC_{vs} is equipped with CMOS RGB Progressive Scan 1/2.9 sensor, and delivers HDTV 1080p video in multiple, individually configurable H.264 and Motion JPEG video streams and has a built-in IR illumination. Moreover, visible camera has $18\times$ optical motorized zoom and auto-focus. The corresponding single frame resolution is 1920×1080 pixel. The TC_{th} provides thermal imaging, with an Uncooled Micro bolometer 384×288 sensor (image can be scaled up to 768×576) and also adopting a noise filter which gives improved thermal image contrast while keeping noise levels low. The system includes a local server which is a HP ProLiant MicroServer Gen 8, two 1 Tb storage drives and a router, model D-Link's Wireless N150 4G LTE for data transmission.

During the installation phase, a collection of reference images for both internal and external calibration tasks are gathered on site. Specifically, intrinsic parameters are estimated by imaging a well-defined pattern from different angles and distances. Checkerboard patterns are typically used for calibration, since they provide easily detectable features, the intersections between the black and white squares form high contrast points, estimated with sub-pixel accuracy. Hence, for visible cameras the pattern used is a classic paper chessboard over a smooth plane, shown in Fig. 7.

For the internal and external calibration of TC_{th} , the use of different emissivity materials is proposed. Since low emissive materials would appear colder than high emissive ones, aluminium foil tape stuck on paper, as highlighted in (Engström et al., 2013) is used (Fig. 8).

Results from the calibration procedure show that the lens deformation is dominated by the radial component, which errors become larger than 30 pixel at the outer edge of the original image, while the



Fig. 6. Cameras location at Torre Canne (TC) and the coastal stretch framed.



Fig. 7. Top: Classic paper chessboard for internal calibration; Bottom: Example of pattern used as GCP for external calibration.

errors related with the tangential component are always lower than 1 *pixel*. The computed average error of re-projection is calculated as always less than 0.52 *pixel*. Camera external orientation is estimated using around 8 ÷ 10 *GCPs*, for each camera, among fixed structures

and a 1 m² chessboard pattern (classic and mixed aluminium/paper) using unique central intersection between squares.

An example of image resolution, explaining the dimension of each pixel in the geographic space, is represented in Fig. 9 for visible camera. It shows the typical contrast between alongshore and cross-shore components.

The near-alongshore footprint is more sensitive to the distance from the camera and ranges from decimetre to around 13 m when the distance is less than 1 km. On the other hand, the near-cross-shore component is generally under the 1 m in the principal target area. By increasing the geo-rectified area would decrease the positional accuracy.

3.2. Torre Lapillo, Porto Cesareo (Lecce, Italy)

3.2.1. Study area

The Marine Area of Porto Cesareo is an interesting site from a morphological point of view. It is constituted by typical sub-environment of low-lying coasts, with calcarenitic rocky and sandy beaches. Sandy beaches are characterized by a mean diameter $D_{50} \sim 0.47$ mm and $D_{95} \sim 1.38$ mm.

Since the first 60's, the number of establishments has been increased, with remarkable damages on the emerged beach, especially for dunes stability. The establishments' managers apply a common defence practice during the spring season, by means of geotextile sandbags which are uniformly distributed just few meters close to coastline, determining a morphological change in shape of the ordinary and stormy berms and reducing shore erosion. It has been revealed that the main reason connected to the erosional trend in the period 2009–2011 could be related to the mean sea level rise (about 13 cm), amplified by significant storms occurred (AdB-Puglia, 2015). Particularly, the shoreline erosional hotspots are located in southeast, where in 2013–2015 the cumulative sediments balance resulted less than -10 m.

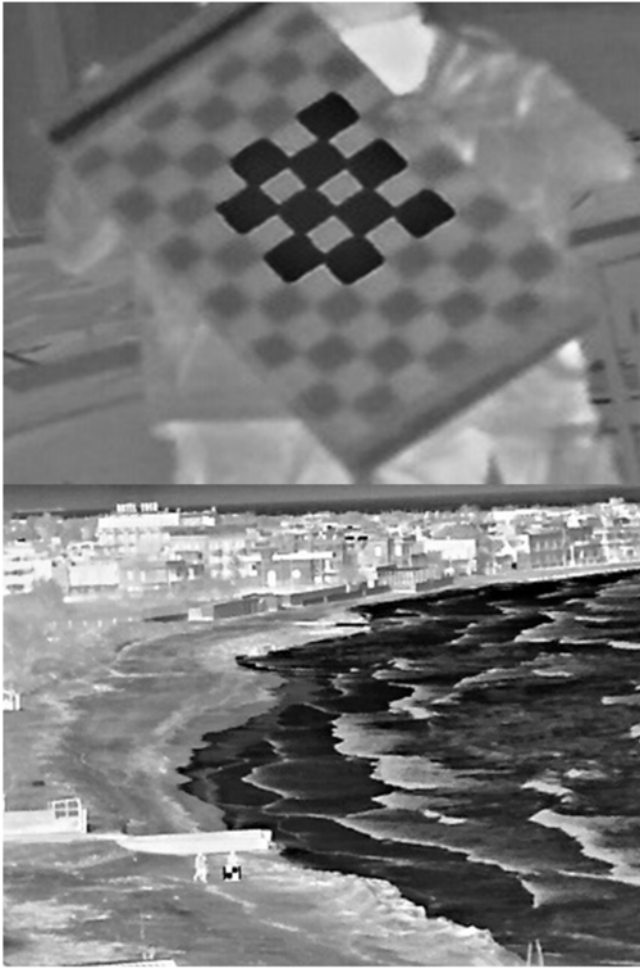


Fig. 8. Top: Paper/Aluminium chessboard for internal calibration; Bottom: Example of pattern used as GCP for external calibration.

For the majority of the time (49.7%) the waves approach from SSE, while for 34.8% they come from SW direction. The wave climate in the area is moderate to low, with an annual significant wave height less than 0.75 m for the 44% of observations in 2006–2013, while a 12.17% for $0.75 < H_s < 1.75$ m and only the 0.66% with $H_s \geq 3.0$ m (AdB-Puglia, 2015). The peak period T_p in the interval $3 \div 5$ s represents the most frequent (31.9% around).

3.2.2. System implementation

At Torre Lapillo (TL), two IP network cameras are installed on a steel pole, fixed on parapet, at the roof of a beach establishment. The approximate orthometric height of the cameras is, in this case, 7.5 m (ITALGEO 2005). The video-station placed at PC (Fig. 10) includes a couple of identical visible cameras (PC_{vs1} , PC_{vs2}). The first one stared at NW direction, with FoV equal to 51.6° , while the second one faced to SE direction, with a FoV of 56.2° . Both are Axis, Mod. Q1765-LE Network Cameras. The same hardware equipment as TC shore is installed.

The pixel accuracy for both cameras in the alongshore component ranges from centimetre to around 14 m when the distance is less than 700 m, while near-cross-shore footprint is generally lower than 2 m. The system accuracy mainly depends on the pixel footprint, the calibration and geo-rectification procedure and stability of camera over time. In order also to evaluate overall new system positional accuracy, 6 GCPs placed at distance from the camera ranging from 10 m

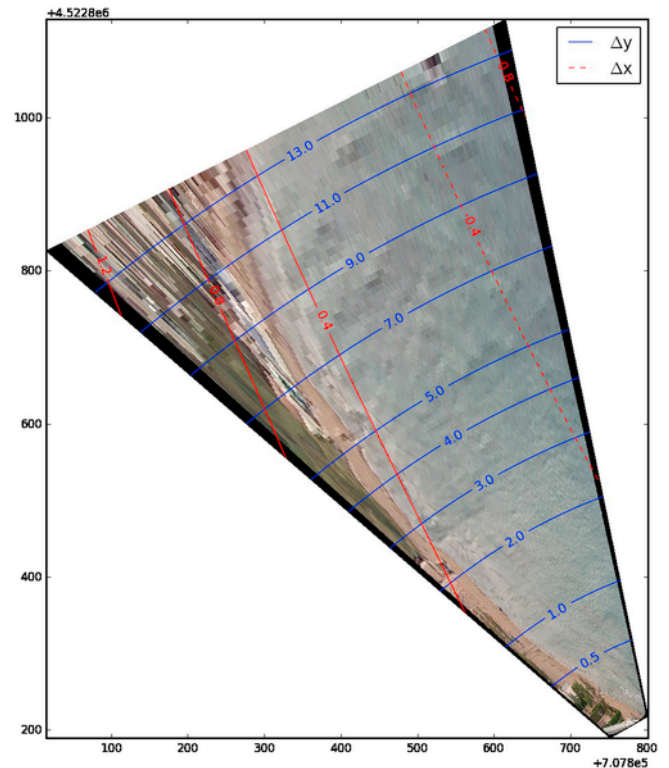


Fig. 9. Pixel footprint components (m) at TC site, along 800 m beach stretch in long-shore (black lines) and cross-shore (red lines) directions. (For interpretation of the references to colour in this figure legend, the reader is referred to the web version of this article.)

to around 300 m are used. Results show significant differences between cross-shore and alongshore positional accuracy, with a Root Mean Square Error (RMSE) of 0.43 m and 5.21 m, respectively. The error is mainly related to the pixel footprint, with the longshore accuracy error that significantly dominate, as expected.

3.3. First results and discussion

The SDM is tested on the new video system at PC, aimed to validate the results, by firstly comparing manual shoreline contours with the automatic extracted ones. The intertidal bathymetry calculated from the SDM is then compared with GPS field surveys.

The model is validated by using 15 Timex images recorded in the first months of system working, representative of main illumination and wave conditions for both cameras. For each analysed image, the displacement between automatic and manual shoreline is evaluated in terms of pixel distance, over several transects (Fig. 11), in order to appropriately calculate the main statistics (i.e. max, min, mean, std. dev.).

Over all the images taken from both cameras, the mean pixel distance is about 1.17 pixel and the mean of maximum values is about 3.77 pixel. All datasets are approximately balanced around 1.2. However, there is substantially more variation in some images datasets with a maximum range from -5.5 to 7.3 , and a minimum range from -1.3 to -0.9 pixel. As for Alimini, in most images the sample dispersion is close to the median. In order to assess the SDM accuracy, results are compared to similar previous experiences which measure the differences between automatic and manual shorelines in pixels (Osorio et al., 2012; Santos et al., 2012), showing a very good agreement. Such a comparison demonstrates that enlarging the image to be processed, by eliminating the ROI area (e.g. used in Santos et al.,



Fig. 10. Cameras location at Torre Lapillo (TL).

2012) or not limiting the contour extraction only on selected cross-shore transects (as in Osorio et al., 2012) does not induce additional errors to the final results, and confirms the high reliability of the proposed SDM, not human-interactive dependant. Moreover, it has to be

noticed that the SDM does not require field instrumentation to correct the detected contour as in Osorio et al., 2012, where one step of correction process is based on a field installed tide gauge. The SDM potentiality is also demonstrated when the routines work on images characterized by some peculiarities, as in example intertidal bars, well recognized by the model. In addition, the shoreline extraction is not influenced by the algae blooms on shoreface, which could interfere with contours detection, leading to errors. Outliers are almost completely associated with the presence of geotextile sandbags and often with illumination conditions at sunrise/sunset. In fact, when the pixel distance between the bags offshore limit and shoreline is less than around 2.5 pixel , the SDM could lead to a single result in that neighbourhood, which propagates in cascade until the last step of correction in the main routine. Further experiments are needed in order to highlight ambiguities in recognizing sharp bends along the shoreline, especially for transects placed at the FoV outer areas, that should be properly taken into account. Moreover, the results show that the SDM algorithm calibrated and validated at Alimini first and then tested at Porto Cesareo, by using the same model calibration parameters, could be easily extended at different sites, characterized by different morphological features and site geographical exposition.

Several authors approach the determination of the intertidal bathymetry of sandy beaches from video system. Previous works, since first experiences of (Aarninkhof et al., 2003; Davidson et al., 2007; Holland et al., 1997), base the intertidal reconstruction on geo-rectified shorelines at elevations derived from site-specific parameterization of the water level referred to the offshore (Uunk et al., 2010) or breaking wave height (Vousdoukas et al., 2011), by applying specific models in order to quantify the set-up and swash contributions.

The process presented hereafter is based on the Digital Elevation Model (DEM) constructed from the geo-rectified time-varying shorelines over a tidal cycle, in quite wave condition, to neglect wave set-up and swash effects. Shorelines extracted from images are geo-rectified with respect to the filtered sea-level measurement, z_{sl} , acquired by the nearest tide-gauge (red point in Fig. 5) belonging to the Apulia Monitoring network, sampled every 15 minutes. With regards to the pixel accuracy introduced in Sub-Sec. 2.2.2, when the system is used for the extraction of intertidal bathymetry, the error related to the



Fig. 11. Example of comparison between manually and automatic shoreline contours with 20 transects overlapped (cam PC_{vs1}).

pixel footprint in the vertical direction is further reduced as foreshore slope is generally about 0.1, with a consequent reduction of the error by an order of magnitude (Silva et al., 2009).

The shoreline contours, automatically stored also as shapefiles for being digitized in GIS environment, are processed by using Triangulated Irregular Network (TIN). A Real Time Kinematic survey using differential GPS solution on the Global Navigation Satellite System (GNSS) of Apulia Region is conducted along the beach stretch monitored until around 300 m from the camera's location, in order to measure the beach profiles over 16 cross-shore transects. The measured profiles are then compared with the intertidal bathymetric profiles extracted from the reconstructed DEM, obtained from video analysis in the same day of the survey.

Fig. 12 highlights the transects positions and few automatic detected shorelines, overlapped on a portion of rectified snapshot image, framed by PC_{vs1} camera FoV.

The Ionian Sea is generally characterized by low tidal amplitude oscillations, ranging from 0.1 ÷ 0.6 m below the still water level. For this reason, due to the mean beach slope equal to about 10%, the mean projected horizontal distance investigated is equal to around 2 m, with a maximum vertical excursion of around 0.2 m.

In Fig. 13 (top), as an example, both measured (solid lines) and calculated (dashed lines) profiles are reported for Transects n. 0, 4, 5 and 11. The comparison shows quite good results, with a mean RMS

error overall transects equal to 0.025 m (Fig. 13, bottom). In particular, the lowest RMS error (equal to about 0.005 m) occurs for Transect n. 11, which is characterized by a straight linear beach profile. It is not observed any uniform decrease trend with the distance, most probably due to a not so large alongshore distance investigated (≤ 300 m). Whereas, the greatest errors (i.e. Transects n. 4, 5 and 6 of about 0.04 m) can be observed when beach profiles present small changes in elevation (\approx cm). The errors, although negligible for morphological analysis purposes, could be substantially attributed to the pixel footprint and geo-rectification errors due to camera geometry inaccuracies. Moreover modest uninform swash motions during Timex production at the beach-face could lead to shoreline points having different elevations with respect to horizontal plane z_{s1} used for geo-rectification and then, the camera perspective may also provoke shadowing effects particularly significant with abrupt topography irregularities (Vousdoukas et al., 2011). Such results seem to be fully comparable with respect to the previous studies performed on beach intertidal bathymetry reconstruction, mainly deployed on beaches characterized by a higher tidal amplitude. In fact, by using Argus system (Aarninkhof et al., 2003), obtained errors lower than 0.15 m along about 2 km long beach. Plant and Holman (1997) reported 0.24 m vertical RMSE, later corrected to 0.06 m when empirical corrections of water level were made and Vousdoukas et al. (2011), using an automated video system with two MOBOTIX cameras, found a vertical RMSE of 0.22 m for a five-month period of fully automation operation.

The efficacy assessment of the procedure adopted for image displacement needs long-term monitoring, but it has been tested in an event of human-accident displacement, during maintenance operations. Consider this, in the 5th step of Section 1.3, the reflection and scaling factors are assumed to be null, since the undistorted images are used and the influence of thermal expansion neglected. Estimated accuracy after the correction is overall below 0.4 pixel, highlighting the robustness and well optimized solution strategy for geometry correction proposed.

4. Conclusions

In the paper, a new video coastal video monitoring system deployed and integrated in the Apulia Region Monitoring Network (South Italy) is presented. Nowadays, risk assessment plays a fundamental role in preventing irreversible erosion processes as well as flooding damages. In this context, the video monitoring represents a low-cost instrument to store a large amount of data, due to the feasibility in extracting several morphodynamic and hydrodynamic measurements from images/videos.

In 2015, two new video monitoring stations, born to work completely automatically were installed at two sites along Apulian coasts, to study both morphodynamic and hydrodynamic processes affecting the coast. For this reason, a new model (SDM) for image processing has been developed, aimed at extracting shoreline from Timex oblique images. The procedure is mainly based on the recognition of sea/sand contour from an automatic segmented area. The SDM has been firstly calibrated and then validated on images derived from different video systems, facing sites characterized by different geographic expositions and illumination conditions. Such a procedure demonstrates the feasibility of the model to be extended at different sites, giving good results in shoreline detection, quantified by comparing manual and automatic shorelines. The SDM model has been firstly developed for such morphological features detection at Alimini's station, located at low altitude, resulting in huge swash areas and characterized by algae blooms that make ambiguous the interface recognition, then it is tested at PC, where the installation of geo-textile sandbags further enhances discontinuity uncertainties. At both

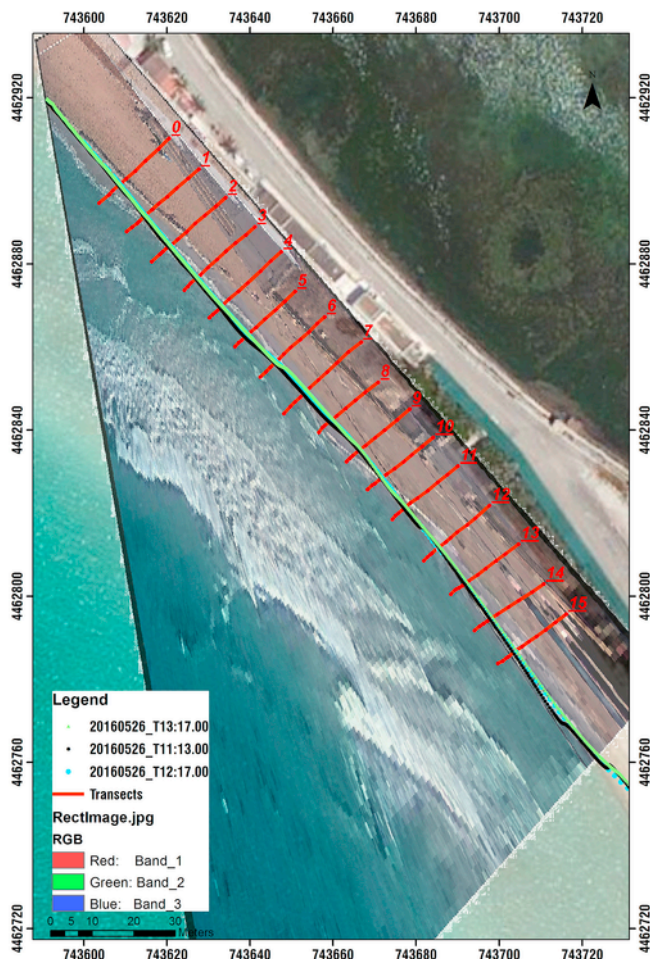


Fig. 12. Cross-shore transects (red pointed GCPs), examples of automatic shorelines overlapped on a snapshot geo-rectified image from camera PC_{vs1} . (For interpretation of the references to colour in this figure legend, the reader is referred to the web version of this article.)

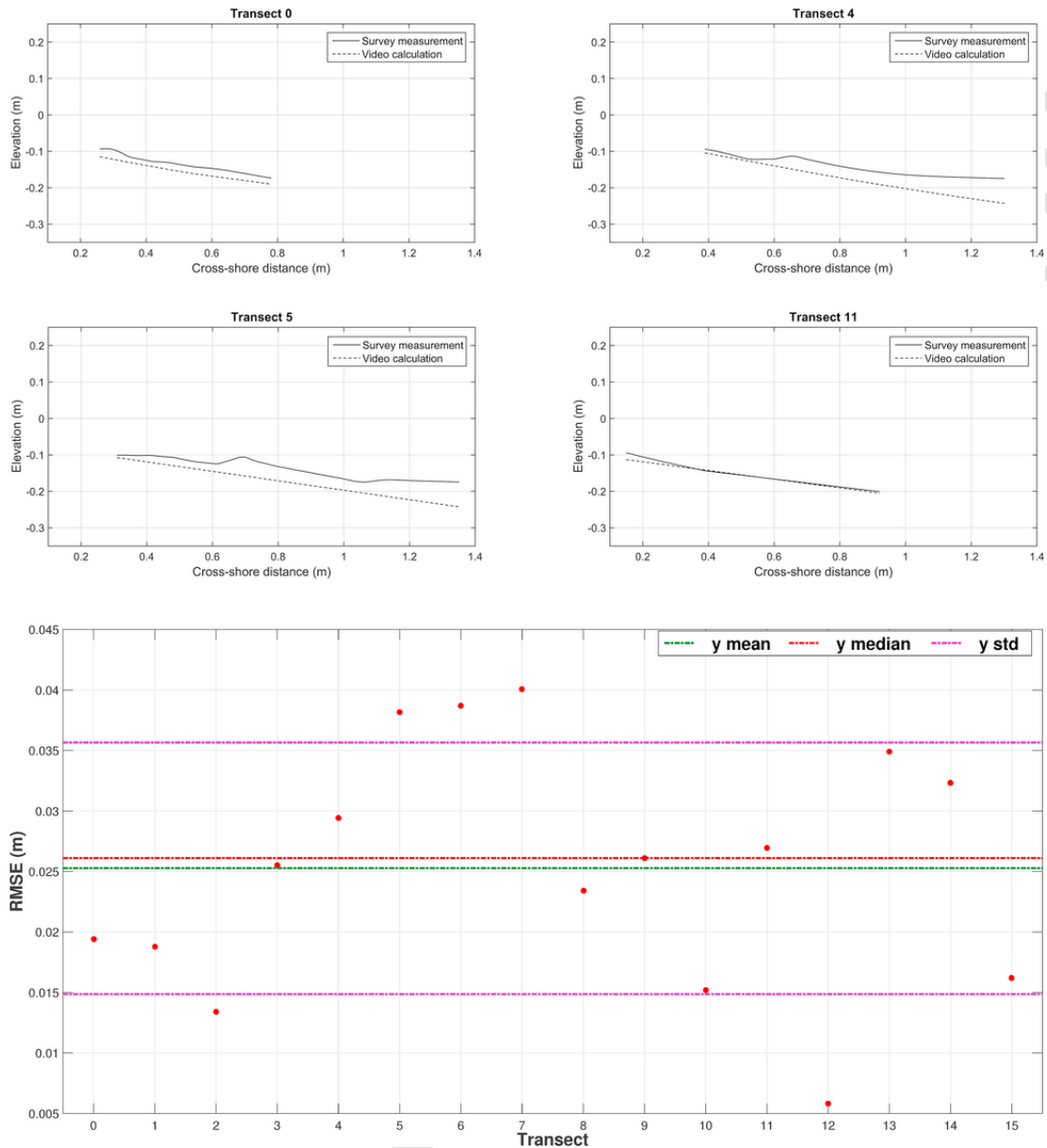


Fig. 13. Top: Comparison of intertidal bathymetry derived from video analysis with the field measured profiles for Transects n. 0, 4, 5 and 11; Bottom: Vertical RMS error (m) for all transects analysed 9.

sites, it leads to quite sound/reliable results, quantified by comparing manual and automatic shorelines. Hence, such a procedure demonstrates the feasibility of the model to be extended at different sites characterized by distinct morphological behaviour, but also geographic expositions and illumination conditions.

Another strength of the system is the dissemination of results on a web portal, freely accessible. In real time, users can view and download for free processed images from all camera installed, shoreline maps with different time intervals and time shoreline variation on user-specified transects, in cross-shore direction. A specific routine has been developed, allowing the automatic geo-rectification of images with respect to the sea level registered by the nearest tide gauge.

Several coastal information can be provided from images. In the present work first results on intertidal bathymetry derived from video analysis is presented. The comparison with D-RTK survey shows a good agreement, with a mean RMS error, overall investigated tran-

sects, equal to 0.025 m. Moreover, a thermal camera has been installed in TC shore mainly for double purposes: (i) support the visible stream during nightlight hours in order to monitor beach, particularly on severe events and (ii) segmentation of the upper part of intertidal area for studies of potential sources of Aeolian sediment (Hoonhout et al., 2013) by using the Global Probability of Boundary method.

Acknowledgements

This research is partially supported by Authority of Basin of Apulia Region (Italy), particularly in the persons of Prof. Antonio Di Santo (Secretary-General), Dott. Nicola Palumbo, and Dott. Roberto Francioso. We thank our colleagues from ACIC (<http://www.acic-tech.be>) who provided expertise in web-application building and management.

References

- Aarninkhof, S.G.J., 2003. Nearshore Bathymetry Derived from Video Imagery. TU Delft, Delft University of Technology.
- Aarninkhof, S.G.J., Ruessink, B.G., Roelvink, J.A., 2005. Nearshore subtidal bathymetry from time-exposure video images. *J. Geophys. Res. Oceans* 110, C06011.
- Aarninkhof, S.G.J., Turner, I.L., Dronkers, T.D.T., Caljouw, M., Nipius, L., 2003. A video-based technique for mapping intertidal beach bathymetry. *Coast. Eng.* 49, 275–289.
- AdB-Puglia, 2015. Relazione tecnica finale: "Monitoraggio delle dinamiche meteo-marine di controllo dei fenomeni di erosione delle coste". (Technical Report).
- Ansar, A., Daniilidis, K., 2003. Linear pose estimation from points or lines. *Pattern Anal. Mach. Intell. IEEE Trans.* 25, 578–589.
- Arbelaez, P., Maire, M., Fowlkes, C., Malik, J., 2011. Contour detection and hierarchical image segmentation. *Pattern Anal. Mach. Intell. IEEE Trans.* 33, 898–916.
- Bay, H., Ess, A., Tuytelaars, T., Van Gool, L., 2008. Speeded-up robust features (SURF). *Comput. Vis. Image Underst.* 110, 346–359.
- Boak, E.H., Turner, I.L., 2005. Shoreline definition and detection: a review. *J. Coast. Res.* 688–703.
- Bouguet, J.Y., 2004. Camera Calibration Toolbox for Matlab.
- Bradski, G., Kaehler, A., 2008. Learning OpenCV: Computer Vision with the OpenCV Library. O'Reilly Media, Inc..
- Damiani, L., Molfetta, M., 2008. In: Damiani, L., Mossa, M. (Eds.), A video based technique for shoreline monitoring in Alimini (LE). *Coastlab08*, pp. 153–156.
- Damiani, L., Aristodemo, F., Saponieri, A., Verbeni, B., Veltri, P., Vicinanza, D., 2011. Full-scale experiments on a beach drainage system: hydrodynamic effects inside beach. *J. Hydraul. Res.* 49, 44–54.
- Davidson, M., Van Koningsveld, M., de Kruijf, A., Rawson, J., Holman, R., Lamberti, A., Medina, R., Kroon, A., Aarninkhof, S., 2007. The CoastView project: developing video-derived Coastal State Indicators in support of coastal zone management. *Coast. Eng.* 54, 463–475.
- Engström, P., Larsson, H., Rydell, J., 2013. Geometric Calibration of Thermal Cameras. pp. 88970C-88970C-88978.
- Estrella, M., Gaventa, J., 1998. Who Counts Reality?: Participatory Monitoring and Evaluation: a Literature Review. Institute of Development Studies Brighton.
- Fiore, P.D., 2001. Efficient linear solution of exterior orientation. *IEEE Trans. Pattern Anal. Mach. Intell.* 140–148.
- Fischler, M.A., Bolles, R.C., 1981. Random sample consensus: a paradigm for model fitting with applications to image analysis and automated cartography. *Commun. ACM* 24, 381–395.
- Gao, X.-S., Hou, X.-R., Tang, J., Cheng, H.-F., 2003. Complete solution classification for the perspective-three-point problem. *Pattern Analysis and Machine Intelligence. IEEE Trans.* 25, 930–943.
- Hartley, R., Zisserman, A., 2003. Multiple View Geometry in Computer Vision. Cambridge university press.
- Holland, K.T., Holman, R.A., Lippmann, T.C., Stanley, J., Plant, N., 1997. Practical use of video imagery in nearshore oceanographic field studies. *IEEE J. Ocean. Eng.* 22, 81–92.
- Holman, R., Plant, N., Holland, T., 2013. cBathy: a robust algorithm for estimating nearshore bathymetry. *J. Geophys. Res. Oceans* 118, 2595–2609.
- Holman, R.A., Stanley, J., 2007. The history and technical capabilities of Argus. *Coast. Eng.* 54, 477–491.
- Hoonhout, B., Baart, F., de Vries, J.v.T., 2013. Intertidal Beach Classification in Infrared Images.
- Hoonhout, B., Radermacher, M., Baart, F., Van der Maaten, L., 2015. An automated method for semantic classification of regions in coastal images. *Coast. Eng.* 105, 1–12.
- Horand, R., Dornaika, F., Lamiroy, B., 1997. Object pose: the link between weak perspective, paraperspective, and full perspective. *Int. J. Comput. Vis.* 22, 173–189.
- IOC, 2006. Manual on Sea Level Measurement and Interpretation. Manuals and Guides 14: an Update to 2006. JCOM Tech. Rept No. 31 Intergovernmental Oceanographic Commission of UNESCO, Paris. http://www.psmsl.org/train_and_info/training/manuals/manual_14_final_21_09_06.pdf. <http://ftp.wmo.int/Documents/PublicWeb/amp/mmop/documents/JCOMM-TR/J-TR-31/JCOMM-TD-31.pdf>.
- Jimenez, J.A., Osorio, A., Marino-Tapia, I., Davidson, M., Medina, R., Kroon, A., Archetti, R., Ciavola, P., Aarninkhof, S.G.J., 2007. Beach recreation planning using video-derived coastal state indicators. *Coast. Eng.* 54, 507–521.
- Kendall, D.G., 1989. A survey of the statistical theory of shape. *Stat. Sci.* 87–99.
- Kingston, K.S., 2003. Applications of Complex Adaptive Systems Approaches to Coastal Systems.
- Kingston, K.S., Mallet, C., Plant, N.G., Davidson, M.A., 2003. Inter-tidal Mapping of Morphological Features from Remotely Sensed Data. Submitted to Marine Geology.
- Kroon, A., Davidson, M.A., Aarninkhof, S.G.J., Archetti, R., Armario, C., Gonzalez, M., Medri, S., Osorio, A., Aagaard, T., Holman, R.A., Spanhoff, R., 2007. Application of remote sensing video systems to coastline management problems. *Coast. Eng.* 54, 493–505.
- Lau, D.L., 1997. Magicwand.c. Mathworks.
- Lisi, I., Molfetta, M., Bruno, M., DiRisio, M., Damiani, L., 2011. Morphodynamic classification of sandy beaches in enclosed basins: the case study of Alimini (Italy). *J. Coast. Res.* 180.
- Lu, C.-P., Hager, G.D., Mjolsness, E., 2000. Fast and globally convergent pose estimation from video images. *Pattern Anal. Mach. Intell. IEEE Trans.* 22, 610–622.
- Nagy, G.J., Gómez-Erache, M., Kay, R., Glavovic, B., Kelly, M., Kay, R., Travers, A., 2015. A risk-based and participatory approach to assessing climate vulnerability and improving governance in coastal Uruguay. *Clim. Change Coast. Build. Resilient commun.* 357–378.
- OpenCV, 2016. Documentation. "Open Source Computer Vision."
- Osorio, A.F., Medina, R., Gonzalez, M., 2012. An algorithm for the measurement of shoreline and intertidal beach profiles using video imagery: PSDM. *Comput. Geosci.* 46, 196–207.
- Pedrycz, W., 1998. Conditional fuzzy clustering in the design of radial basis function neural networks. *neural networks. IEEE Trans* 9, 601–612.
- Pele, O., Werman, M., 2010. The Quadratic-chi Histogram Distance Family, European Conference on Computer Vision. Springer, 749–762.
- Penate-Sanchez, A., Andrade-Cetto, J., Moreno-Noguer, F., 2013. Exhaustive linearization for robust camera pose and focal length estimation. *Pattern Anal. and Mach. Intell. IEEE Trans* 35, 2387–2400.
- Petrillo, L.d.I.d.C., 2010. In: Chimica, D.d.I.d.A.e.d. (Ed.), Determinazione del clima meteorologico al largo e sottocosta e del trasporto solido per paraggi significativi della costa pugliese. (Bari).
- Plant, N.G., Aarninkhof, S.G., Turner, I.L., Kingston, K.S., 2009. The Performance of Shoreline Detection Models Applied to Video Imagery.
- Plant, N.G., Holman, R.A., 1997. Intertidal beach profile estimation using video images. *Mar. Geol.* 140, 1–24.
- Quartel, S., Addink, E., Ruessink, B., 2006. Object-oriented extraction of beach morphology from video images. *Int. J. Appl. Earth Observ. Geoinform.* 8, 256–269.
- Radermacher, M., Wengrove, M., Van Thiel de Vries, J., Holman, R., 2014. Applicability of video-derived bathymetry estimates to nearshore current model predictions. In: Proceedings of the 13th International Coastal Symposium, Durban, South Africa, 13-17 April 2014. *Journal of Coastal Research, Special Issue* 70, 2014. Coastal Education and Research Foundation (CERF).
- Rigos, A., Andreadis, O., Andreas, M., Voudoukas, M., Tsekouras, G., Velegrakis, A., 2014. Shoreline extraction from coastal images using Chebyshev polynomials and RBF neural networks. In: Iliadis, L., Maglogiannis, I., Papadopoulos, H. (Eds.), Artificial Intelligence Applications and Innovations. Springer Berlin Heidelberg, pp. 593–603.
- Santos, F., Pais-Barbosa, J., Teodoro, A.C., Gonçalves, H., Baptista, P., Moreira, A., ... Neves-Santos, F., 2012. Coastal morphodynamic features/patterns analysis through a video-based system and image processing. In: SPIE Remote Sensing. International Society for Optics and Photonics (pp. 85381Q-85381Q).
- Saponieri, A., Damiani, L., 2015. Numerical analysis of infiltration in a drained beach. *Int. J. Sustain. Dev. Plan.* 10, 467–486.
- Semiring, L.E., 2015. Rip Current Prediction System for Swimmer Safety: towards Operational Forecasting Using a Process Based Model and Nearshore Bathymetry from Video. TU Delft, Delft University of Technology.
- Silva, A., Taborda, R., Catalão, J., Freire, P., 2009. DTM extraction using video-monitoring techniques: application to a fetch limited beach. *J. Coast. Res.* 203–207.
- Simarro, G., Bryan, K.R., Guedes, R.M., Sancho, A., Guillen, J., Coco, G., 2015. On the use of variance images for runup and shoreline detection. *Coast. Eng.* 99, 136–147.
- Stockdon, H.F., Holman, R.A., Howd, P.A., Sallenger Jr., A.H., 2006. Empirical parameterization of setup, swash, and runup. *Coast. Eng.* 53, 573–588.
- Thévenaz, P., Sage, D., Unser, M., 2012. Bi-exponential edge-preserving smoother. *Image Proc. IEEE Trans.* 21, 3924–3936.
- Turner, I.L., Leyden, V.M., Symonds, G., Mcgrath, J., Jackson, A., Jancar, T., Aarninkhof, S., Elshoff, I., 2001. Predicted and observed coastline changes at the Gold Coast artificial reef. In: Coastal Engineering Conference. ASCE American Society of Civil Engineers. pp. 1836–1847.
- Uunk, L., Wijnberg, K., Morelissen, R., 2010. Automated mapping of the intertidal beach bathymetry from video images. *Coast. Eng.* 57, 461–469.
- Valipour, M., Banihabib, M.E., Behbahani, S.M.R., 2013. Comparison of the ARMA, ARIMA, and the autoregressive artificial neural network models in forecasting the monthly inflow of Dez dam reservoir. *J. Hydrol.* 476, 433–441.
- Valipour, M., 2016. Variations of land use and irrigation for next decades under different scenarios. *IRRIGA* 1 (01), 262–288.
- Valipour, M., Sefidkouhi, M.A.G., Raeini, M., 2017. Selecting the best model to estimate potential evapotranspiration with respect to climate change and magnitudes of extreme events. *Agric. Water Manag.* 180, 50–60.
- Voudoukas, M., Ferreira, P., Almeida, L., Dodet, G., Psaros, F., Andriolo, U., Taborda, R., Silva, A., Ruano, A., Ferreira, ., 2011. Performance of intertidal topography video monitoring of a meso-tidal reflective beach in South Portugal. *Ocean. Dyn.* 61, 1521–1540.
- Wolf, P.R., Dewitt, B.A., 2000. Elements of Photogrammetry: with Applications in GIS. McGraw-Hill, New York.
- Zhang, Z., 2000. A flexible new technique for camera calibration. *pattern analysis and machine intelligence. IEEE Trans.* 22, 1330–1334.